Electronic Supplementary Information

Spatial Engineering of $Co(OH)_x$ Encapsulated *p*-Cu_2S/*n*-$BiVO_4$ Photoanode: Simultaneously Promoting Charge Separation and Surface Reaction Kinetics in Solar Water Splitting

Bing He,[‡,a] Yang Wang,[‡,ab] Xueqin Liu,*[a] Yinchang Li,[a] Xiaoqin Hu,[a] Jing Huang,[a] Yongsheng Yu,[c] Zhu Shu,[a] Zhen Li,*[a] and Yanli Zhao*[b]

[a]*Engineering Research Center of Nano-Geomaterials of Ministry of Education, Faculty of Materials Science and Chemistry, China University of Geosciences, Wuhan, Hubei 430074, P. R. China*

[b]*Division of Chemistry and Biological Chemistry, School of Physical and Mathematical Sciences, Nanyang Technological University, 21 Nanyang Link, 637371, Singapore*

[c]*College of Chemistry and Chemical Engineering, Xinyang Normal University, Xinyang, Henan 464000, P. R. China*

[‡]*These authors contributed equally.*

E-mail: liuxq@cug.edu.cn, zhenli@cug.edu.cn, zhaoyanli@ntu.edu.sg

Experimental section

Preparation of worm-like $BiVO_4$ electrode

The $BiVO_4$ photoanode was fabricated by an electrodeposition method. First, $Bi(NO_3)_3$ solution (15 mM) was prepared by dissolving $Bi(NO_3)_3 \cdot 5H_2O$ in 0.4 M KI and 30 mM lactic acid solution (50 mL, pH = 1.8, adjusted by HNO_3 solution). Ethanol (20 mL) containing *p*-benzoquinone (46 mM) was slowly added into the $Bi(NO_3)_3$ solution, and the obtained mixture was vigorously stirred for 20 min. Then, the electrodeposition in the prepared electrolyte was carried out in a typical three-electrode system, with a piece of FTO (3 × 1 cm^2) working electrode (WE), a saturated Ag/AgCl reference electrode (RE) and a platinum foil (1.5 × 1.5 cm^2) counter electrode (CE). Cathodic deposition was conducted potentiostatically at -0.35 V vs. Ag/AgCl for 30 s and -0.1 V *vs.* Ag/AgCl at room temperature for 1200 s. The obtained orange BiOI precursor was rinsed with pure water and then dried with N_2. Next, the BiOI precursor was converted to $BiVO_4$ by placing DMSO solution (0.1 mL) containing $VO(acac)_2$ (0.2 M) on the BiOI electrode (1 × 2 cm^2) and heating in a muffle furnace at 450 ºC (ramping rate = 2 ºC min^{-1}) for 2 h to obtain $BiVO_4$. Excess V_2O_5 presented in the $BiVO_4$ electrode was removed by soaking them in NaOH solution (1 M) for 5 min with mild stirring. The resulting worm-like $BiVO_4$ electrode was rinsed with pure water and dried in air.[1]

Preparation of $Cu_2S/BiVO_4$ composite electrode

$Cu_2S/BiVO_4$ composite was synthesized by a successive ionic layer adsorption and reaction (SILAR) method.[2] The saturated CuCl aqueous solution and Na_2S (5 mM) were used to fabricate Cu_2S NP decorated $BiVO_4$ electrode. To control the deposition amount of Cu_2S, the electrode was immersed in solution for 10, 20, 30 and 40 s (recorded as 1-$Cu_2S/BiVO_4$, 2-$Cu_2S/BiVO_4$, 3-$Cu_2S/BiVO_4$ and 4-$Cu_2S/BiVO_4$, respectively). Taking 20 s as an example, the $BiVO_4$ electrode was firstly immersed in the CuCl solution for 20 s to adsorb Cu^+ on the surface of $BiVO_4$ electrode, followed by washing with pure water for 60 s. The sample was then immersed in the Na_2S solution for another 20 s to promote the reaction of S^{2-} with the adsorbed Cu^+ on the surface of $BiVO_4$ electrode and rinsed again with pure water for 60 s.

The resulting $Cu_2S/BiVO_4$ composite photoanode was washed with pure water and dried in air.

Deposition of $Co(OH)_x$ on $Cu_2S/BiVO_4$ composite electrode (CCB)

The outmost $Co(OH)_x$ layer on the photoelectrode was also prepared using the SILAR method.[3] The $Cu_2S/BiVO_4$ composite structure was successively immersed into $Co(CH_3COO)_2$ aqueous solution (100 mL, 50 mM), pure water, NaOH aqueous solution (100 mL, 100 mM), and pure water each for 60 s to finish one cycle deposition of the $Co(OH)_x$ layer. In order to obtain the optimal amount of $Co(OH)_x$ layer, the above SILAR cycle was repeated for 1, 3, 5 and 7 times, and the corresponding samples are recorded as 1-CCB, 3-CCB, 5-CCB, and 7- CCB, respectively.

Characterizations

The obtained products were characterized by a Bruker D8 Advanced X-ray diffractometer (XRD, Bruker AXS D8-Focus). The morphology and size of the materials were characterized by a field-emission scanning electron microscope (FESEM, SU8010) associated with an X-ray energy-dispersive spectrometer (EDS). Transmission electron microscopy (TEM, Talos F200S) images were visualized using a transmission electron microscope at an acceleration voltage of 120 kV. The light absorption properties of as-prepared samples were measured by a UV-Vis diffuse reflectance spectrometer (UV-2550PC spectrophotometer). The photoluminescence measurements were carried out using a Fluoromax 4P spectrofluorometer (Horiba) with a laser (λ = 380 nm) at room temperature. The surface bonding information was analyzed by X-ray photoelectron spectroscopy (XPS, Physical Electronics PHI 1600 ESCA).

Photoelectrochemical (PEC) measurements

The PEC measurements of pure $BiVO_4$, $Cu_2S/BiVO_4$ and CCB composite structures were all achieved with an electrochemical workstation (CHI 650E) in a standard three-electrode system. The photoanodes (pure $BiVO_4$, $Cu_2S/BiVO_4$ and CCB), a platinum foil (1.5 × 1.5 cm^2) and a saturated Ag/AgCl electrode were acted as the WE, CE and RE, respectively. The

simulated solar illumination was by a 150 W Xenon arc lamp with an AM 1.5G filter (100 mW cm^{-2}), and phosphate buffer solution (KPi, 0.5 M, pH = 10) with or without sodium sulfite (Na_2SO_3, 1 M) was used as the electrolyte after N_2 bubbling for 0.5 h.

The current density-potential (J-V) curves were obtained by scanning with continuous voltage changes from -1 V to 1 V *vs.* Ag/AgCl at a scan rate of 10 mV s^{-1}. The measured potentials were converted to the reversible hydrogen electrode (RHE) using the Nernst equation: $E_{RHE} = E_{Ag/AgCl} + 0.059 \times pH + E^0_{Ag/AgCl}$, where E_{RHE} is the converted potential *vs.* RHE, $E_{Ag/AgCl}$ is experimentally measured potential against Ag/AgCl reference electrode, and $E^0_{Ag/AgCl}$ = 0.1976 V (*vs.* Ag/AgCl) at 25 °C.[4]

IPCE was measured at 1.23 V_{RHE} in the same electrolyte and three-electrode setup mentioned above. A solar simulator (300 W Xe arc lamp) and a monochromator were coupled to scan the wavelength of the incident light.

The Mott-Schottky plots were obtained at an amplitude of 10 mV and a frequency of 10^3 Hz. Electrochemical impedance spectroscopy (EIS) was investigated by applying a small AC amplitude of 50 mV and a frequency range from 10^4 to 10^{-2} Hz at open circuit potential.

The H_2 generation rate was determined in an airtight N_2 flow system equipped using a GC7920 gas chromatography. Before the measurement, the system was flowed with N_2 for several hours to remove residual air. The photoanodes were immersed in a mildly stirred KPi solution (0.5 M, pH 10) under AM 1.5G illumination at a bias of 1.23 V_{RHE}.

Calculations

Incident photon-to-electron conversion efficiency (IPCE)

IPCE was calculated by the following equation:[5]

$$IPCE = \frac{1240 \times I(mA \cdot cm^{-2})}{P_{light}(mW \cdot cm^{-2}) \times \lambda(nm)} \times 100\%$$

where λ is the wavelength of incident light, I is the measured photocurrent density at specific wavelength, and P_{light} is the measured light power density at that wavelength (100 mW cm^{-2}).

Applied bias photon-to-current efficiency (ABPE)

ABPE was calculated from the *J-V* curve shown in Fig. 3a. Assuming 100% Faradaic efficiency, the value of ABPE was obtained by the following equation: [5]

$$ABPE = \frac{I(mA \cdot cm^{-2}) \times (1.23 - V_{bias})(V)}{P_{light}(mW \cdot cm^{-2})} \times 100\%$$

where I is the photocurrent density at specific potential, V_{bias} is the applied bias between WE and RHE, and P_{light} is the incident illumination power density (100 mW cm^{-2}).

Charge separation efficiency

The photocurrent density under sulfite oxidation conditions was calculated by the following formula:

$$J_{PEC} = J_{abs} \times \eta_{bulk} \times \eta_{surface}$$

where J_{abs} represents the photocurrent density, which is the value obtained by the electrodes thoroughly converting the absorbed photons to current. The J_{abs} of $BiVO_4$ and $Cu_2S/BiVO_4$ were 5.62 mA cm^{-2} and 6.18 mA cm^{-2}, which were calculated by overlapped area integration of standard solar absorption spectrum and UV-Vis absorption spectrum, respectively (Fig. S5). η_{bulk} (relating to bulk charge separation) and $\eta_{surface}$ (relating to surface reaction kinetics) could be determined by using the flowing formulas: [6]

$$\eta_{bulk} = \frac{J_{sulfite}}{J_{abs}} \times 100\%$$

$$\eta_{surface} = \frac{J_{water}}{J_{sulfite}} \times 100\%$$

where $J_{sulfite}$ and J_{water} are the photocurrent density in the electrolyte with and without sulfite oxidation shown in Fig. 3a,f, respectively.

Carrier density (Nd) through the Mott-Schottky plots

The *Nd* of the obtained photoanode could be roughly estimated through the following equation:

$$Nd = \frac{2}{e_0 \varepsilon \varepsilon_0}\left[\frac{d(1/C^2)}{dv}\right]^{-1}$$

where ε_0 is the permittivity of free space (8.85 × 10^{-12} F m^{-1}), ε is the dielectric constant of

$BiVO_4$ (68),[7] e_0 is electron charge (1.60 × 10^{-19} C), and $d(1/C^2)/d\upsilon$ is the slope of the curve shown in Mott-Schottky plots (Fig. 4d).

Band gap (Eg), valence band (VB) position and conduction band (CB) position

The band gap of semiconductor could be estimated based on the absorption spectrum using the following equation:

$$\alpha = A(h\nu - Eg)^{1/2}/h\nu$$

where α is the diffuse reflectance we measured, $A=log(1/R)$, which R is diffuse reflectance, and $h\nu = hc/\lambda = 1240/\lambda$.

As shown in Fig. S5b, d, $h\nu$ as the abscissa, $(\alpha h\nu)^2$ as the ordinate, the intersection of the tangent, and the X-axis is Eg, the optical band gap of pure $BiVO_4$, $Cu_2S/BiVO_4$ and CCB is 2.46, 2.43 and 2.42 eV, respectively.

Valence band (VB) position and conduction band (CB) position were calculated using the absolute electronegativity value of the semiconductor *via* equations as follows:

$$E_{VB} = X - E_e + 1/2E_g$$

$$E_{CB} = E_{VB} - E_g$$

The value of the absolute electronegativity X in the formula was calculated from the geometric mean of the absolute electronegativity of the atoms in the semiconductor. The values of $BiVO_4$ and Cu_2S are 6.04 and 5.00, respectively.[8] E_e is the energy of free electrons on the hydrogen scale (~4.50 eV). Bringing these parameters into the above equations, the VB positions of $BiVO_4$ and Cu_2S are 2.76 eV and 1.12 eV, and the CB positions are 0.31 eV and -0.13 eV, respectively.

Lifetime of the photogenerated carriers (τ_n)

The lifetime of the photogenerated carriers (τ_n) obtained from the OCVD was calculated by the equation:

$$\tau_n = -\frac{k_B T}{e}\left(\frac{dOCP}{dt}\right)^{-1}$$

where τ_n is the carrier lifetime, k_BT is the thermal energy, and e is the positive element charge. The carrier lifetime could be quantified for the comparison of the charge recombination rate in the junction.

Additional figures and discussions

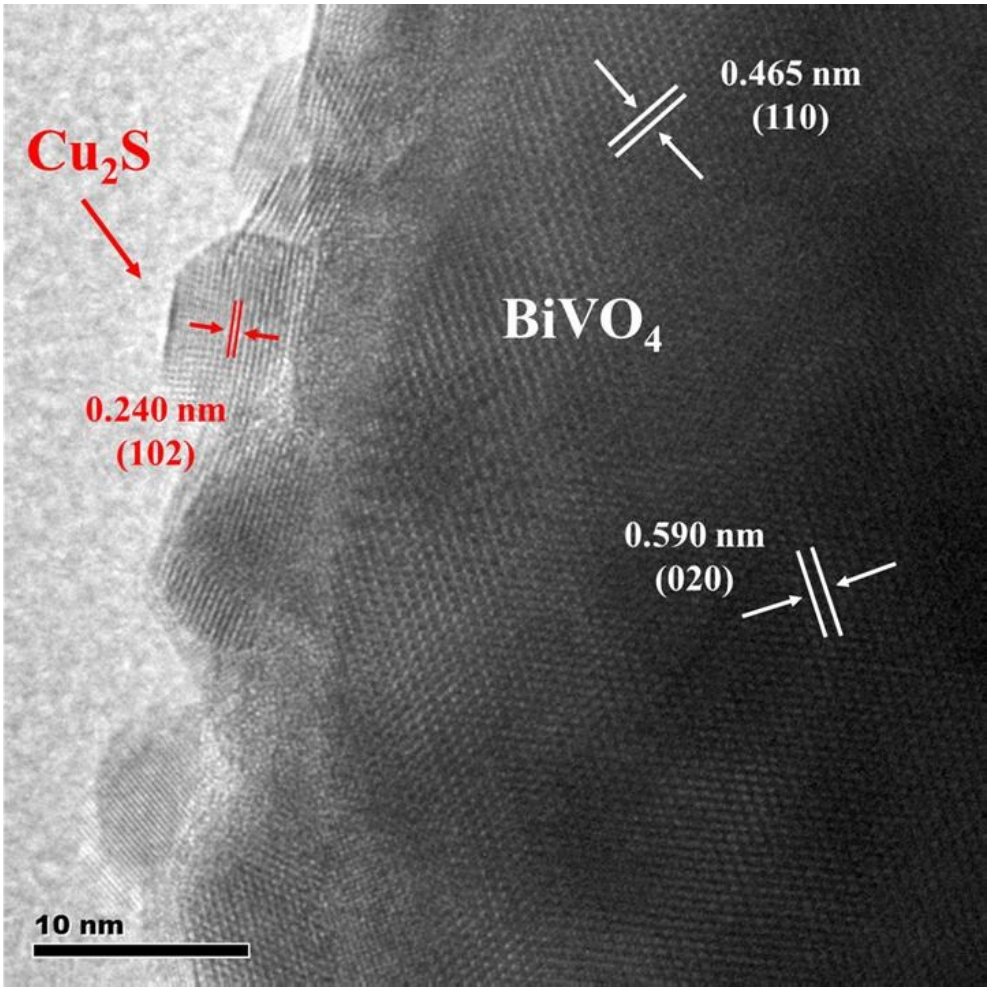

Fig. S1 HRTEM image of $Cu_2S/BiVO_4$.

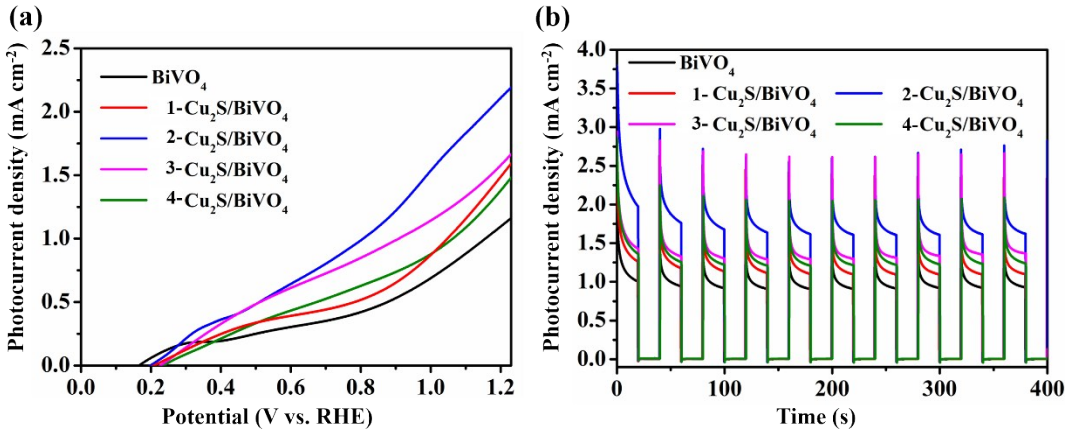

Fig. S2 (a) LSV curves and (b) J-t curves measured at 1.23 V_{RHE} under chopped AM 1.5G in KPi (pH = 10) of $Cu_2S/BiVO_4$ with different Cu_2S NP loading amounts.

The effect of the deposition amount of Cu_2S NPs, controlled by immersion time, on the PEC performance of *p*-Cu_2S/*n*-$BiVO_4$ heterojunction was investigated in detail, as shown in Fig. S2. The highest photocurrent of 2.19 mA cm^{-2} at 1.23 V_{RHE} was achieved by 2-$Cu_2S/BiVO_4$ (*i.e.*, the sample prepared by immersion time of 20 s). With further increase of immersion time, the surface of $BiVO_4$ was attached by excessive Cu_2S NPs, becoming new recombination sites of electrons and holes. In general, the catalytic activity of a *p*-*n* heterojunction photoanode is closely related to the amount and dispersion of its outer *p*-type semiconductors.

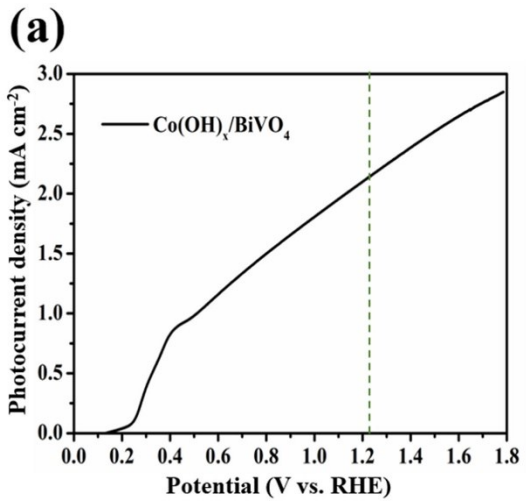

Samples	J (mA cm^{-2})
$BiVO_4$	1.16
$Cu_2S/BiVO_4$	2.19
$Co(OH)_x/BiVO_4$	**2.14**
CCB	3.51

Fig. S3 (a) LSV curve and AM 1.5G in KPi solution (pH = 10) for $Co(OH)_x/BiVO_4$ and (b) photocurrent density for different samples in KPi solution at 1.23 V vs RHE.

After integrating Cu_2S and $Co(OH)_x$, the onset potential of CCB showed a slightly positive shift less than ~30 mV. The slight shift may be due to the interface resistance of the outer loading layer. Upon increasing the bias potential, this shift disappeared and the photocurrent density increased significantly.

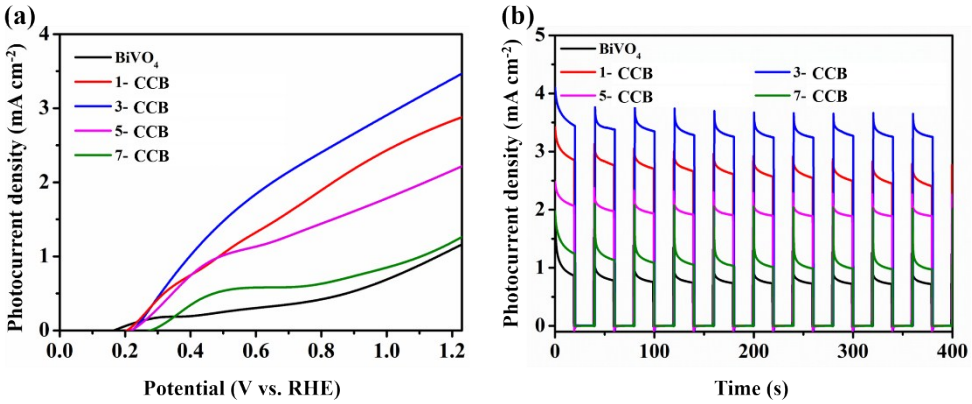

Fig. S4 (a) LSV curves and (b) J-t curves measured at 1.23 V_{RHE} under chopped AM 1.5G in KPi (pH = 10) of CCB with different $Co(OH)_x$ loading amounts.

The PEC performance of CCB photoanode is significantly affected by the $Co(OH)_x$ content, as shown in Fig. S4. Compared to the bare $BiVO_4$ photoanode, all CCB electrodes exhibit remarkably improved photo-induced current density, indicating the efficient modification to the $BiVO_4$ photoanode *via* the simultaneous introduction of *p*-type Cu_2S NPs and $Co(OH)_x$ OECs. Specifically, when the SILAR cycle was increased from 1 to 3 times, the photocurrent increased obviously. However, when the SILAR cycle was increased further to 5 or 7 times, the photocurrents decreased, presumably because the excess $Co(OH)_x$ would increase the transfer resistance of photo-induced holes. Consequently, to maximize the synergistic effect of *p-n* heterojunction and $Co(OH)_x$ in CCB photoanode, the optimal immersion time for Cu_2S NPs and immersion cycle time for $Co(OH)_x$ are 20 s and 3 times, respectively. At this condition, the highest photocurrent density of 3.51 mA cm^{-2} at 1.23 V_{RHE} was obtained for the CCB photoanode.

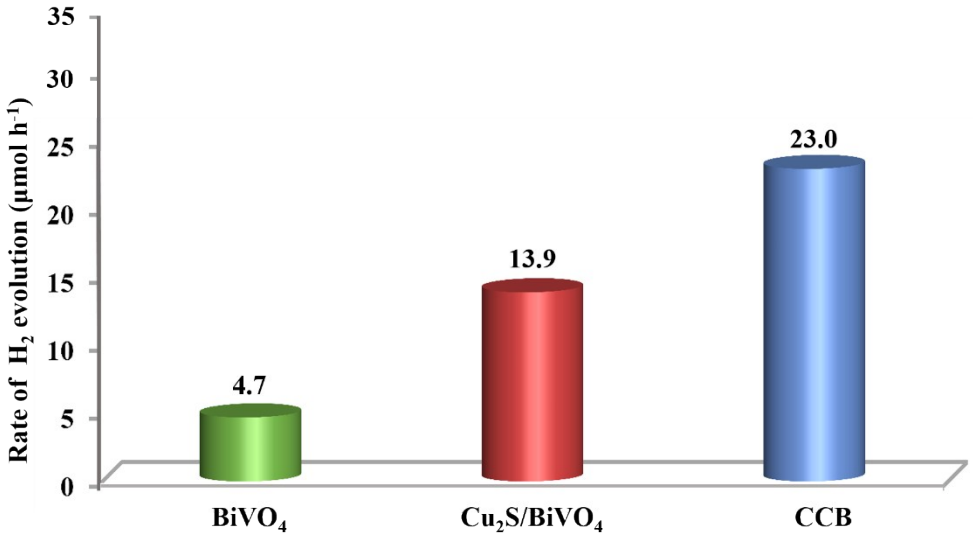

Fig. S5 Rate of H_2 evolution for $BiVO_4$, $Cu_2S/BiVO_4$ and CCB.

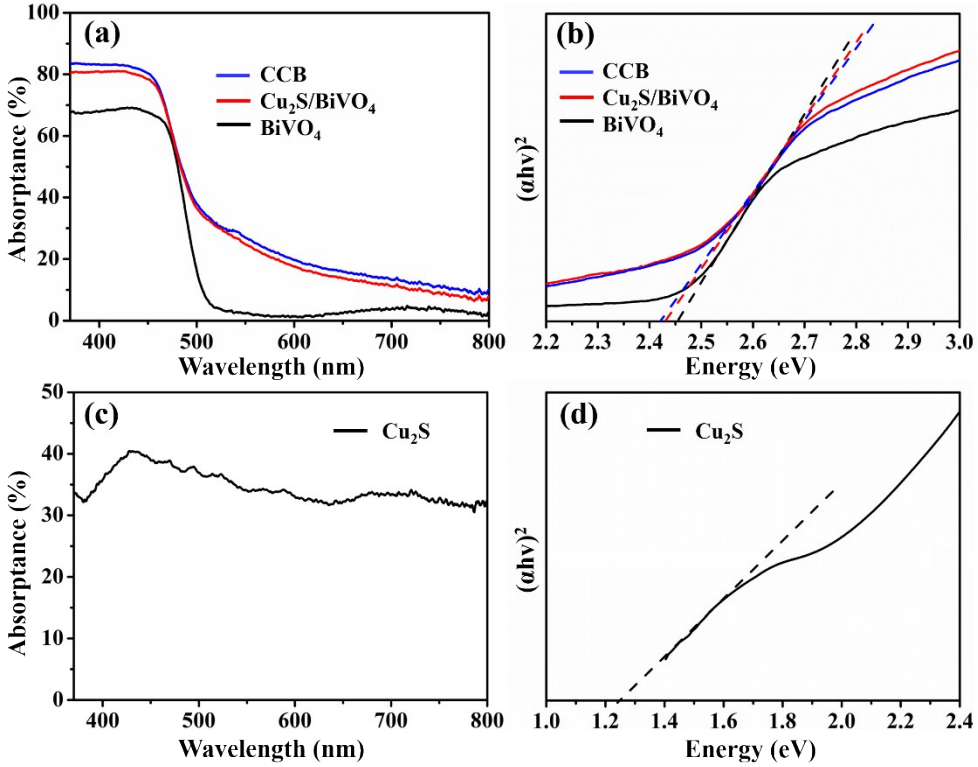

Fig. S6 (a) UV-Vis absorptance spectra and (b) Tauc plots of $BiVO_4$, $Cu_2S/BiVO_4$ and CCB photoanodes. (c) UV-Vis absorptance spectrum and (d) Tauc plot of Cu_2S NPs.

The optical absorption properties of the obtained samples were characterized by UV-Vis diffuse reflectance spectroscopy, as shown in Fig. S6. Bare $BiVO_4$ electrode shows an absorbance edge at ~520 nm (Fig. S6a), corresponding well to the band gap of 2.4-2.5 eV.[9] After the deposition of Cu_2S NPs, the $Cu_2S/BiVO_4$ heterojunction exhibits the extension of light absorption in the visible light wavelength, which is attributed to the narrow band gap of Cu_2S (Eg = 1.25 eV), as shown in Fig. S6d. The CCB electrode displays a similar absorption curve to that of $Cu_2S/BiVO_4$, implying the weak light absorption of ultrathin $Co(OH)_x$ film.

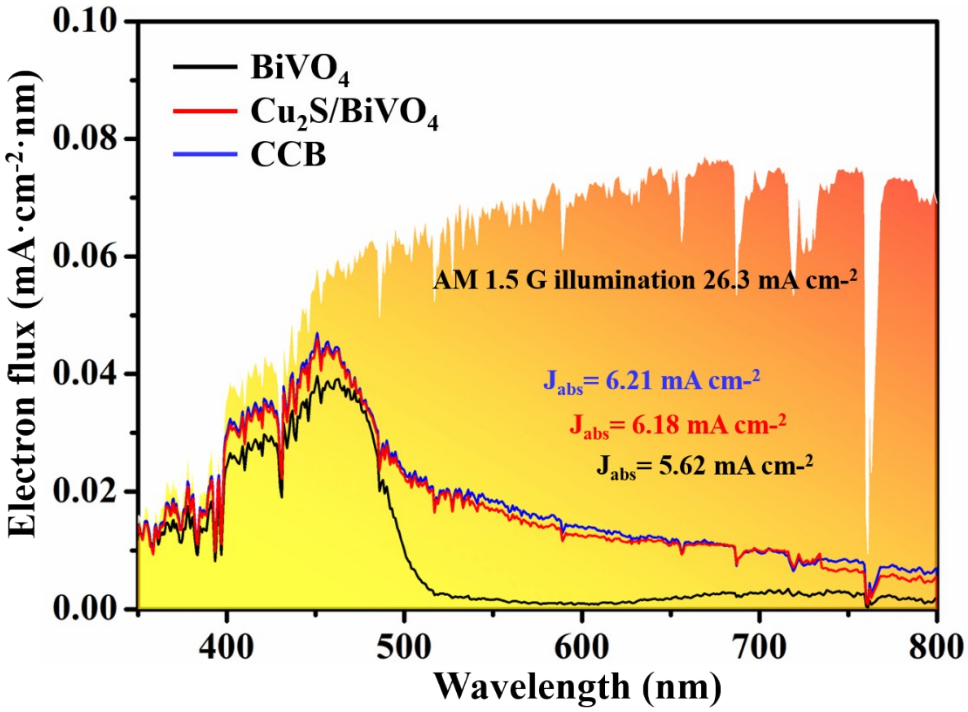

Fig. S7 Electron flux of AM 1.5G solar spectrum, $BiVO_4$, $Cu_2S/BiVO_4$ and CCB photoanodes.

(a)

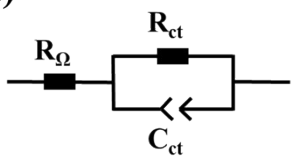

(b)

Samples	R_{Ω}(Ω)	R_{ct}(Ω)	CPE1–T	CPE1–P
$BiVO_4$	27.1	7350	1.8×10^{-4}	0.72
$Cu_2S/BiVO_4$	21.7	2800	1.9×10^{-4}	0.77
CCB	20.1	450	2.7×10^{-4}	0.70

Fig. S8 (a) Randles equivalent circuit model and (b) fitting results of R_{Ω}, R_{ct}, CPE1-T and CPE1-P for different samples in KPi solution without Na_2SO_3 by ZVIEW.

The EIS Nyquist plots for all these photoanodes could be assigned to the series resistance (R_{Ω}) and the interfacial charge transfer resistance (R_{ct}) of the electrode/electrolyte boundary with the Randles equivalent circuit model (Fig. S8). Clearly, the radius of pure $BiVO_4$ photoanode is much larger than that of *p*-Cu_2S/*n*-$BiVO_4$ heterojunction electrode, indicating that the *p*-*n* heterojunction effectively reduces the interface resistance and facilitates the transfer of photogenerated holes. After the coating of $Co(OH)_x$, R_{ct} of CCB decreases significantly, suggesting that, as a water oxidation kinetic catalyst, $Co(OH)_x$ in the composite electrode improves the hole transfer dynamics effectively.

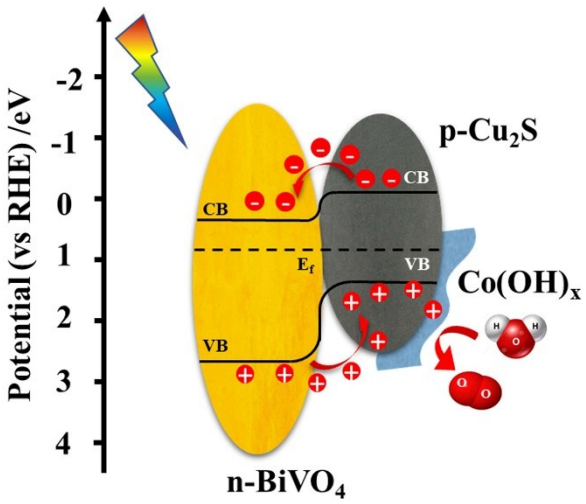

Fig. S9 Proposed band diagram and mechanism of charge separation for CCB.

Tab. S1. Comparison of the solar-driven photoactivity for water oxidation of the current photoanodes with the reported most active $BiVO_4$-based photoanodes prepared by different methods based on the photocurrent density J (mA cm^{-2}) obtained at 1.23 V under AM 1.5G, 100 mW cm^{-2} illumination.

Photoanode	Electrolyte	J (mA cm^{-2})	Ref.
FTO/$BiVO_4$/Cu_2S/$Co(OH)_x$	0.5 M KPi (pH 10)	~3.51	this work
FTO/$BiVO_4$/$ZnFe_2O_4$/Co^{2+}	0.1 M KOH (pH 13)	~2.84	10
FTO/$BiVO_4$/$CoFe_2O_4$	0.5 M Na_2SO_4(pH 7.3)	~0.65	11
FTO/$BiVO_4$/FeF_2	0.5 M Na_2SO_4	~2.49	12
FTO/$BiVO_4$/Cu_2O	0.1 M PBS (pH 7)	~1.72	7
FTO/$BiVO_4$/NiB	0.5 M KBi (pH 9.5)	~4.82	13
FTO/ $BiVO_4$/AgO_x/NiO_x	0.5 M KBi (pH 9.25)	~2.05	14
FTO/$BiVO_4$/FeOOH/NiOOH	1 M KBi (pH 9.5)	~5.31	15
FTO/$BiVO_4$/CoBi	1 M KBi (pH 9.5)	~3.20	10
FTO/$BiVO_4$/Co_3O_4	0.5 M KPi (pH 7)	~2.71	8
FTO/$BiVO_4$/ LDH/ CdTe-QD	0.1 M KPi (pH 7)	~2.23	16

References

1 T. W. Kim and K. S. Choi, *Science*, 2014, **343**, 990−994.

2 K. Guo, Z. Liu, C. Zhou, J. Han, Y. Zhao, Z. Liu, Y. Li, T. Cui, B. Wang and J. Zhang, *Appl. Catal. B: Environ.*, 2014, **154−155**, 27−35.

3 M. Liao, J. Feng, W. Luo, Z. Wang, J. Zhang, Z. Li, T. Yu and Z. Zou, *Adv. Funct. Mater.*, 2012, **22**, 3066−3074.

4 B. Zhang, L. Wang, Y. Zhang, Y. Ding and Y. Bi, *Angew. Chem., Int. Ed. Engl.*, 2018, **57**, 2248−2252.

5 R. Tang, S. Zhou, Z. Yuan and L. Yin, *Adv. Funct. Mater.*, 2017, **27**, 1701102.

6 Y. Wang, F. Li, X. Zhou, F. Yu, J. Du, L. Bai and L. Sun, *Angew. Chem., Int. Ed.*, 2017, **56**, 6911−6915.

7 S. Bai, J. Liu, M. Cui, R. Luo and J. He, A. Chen, *Dalton Trans*, 2018, **47**, 6763−6771.

8 X. Chang, T. Wang, P. Zhang, J. Zhang, A. Li and J. Gong, *J. Am. Chem. Soc.*, **2015**, 137, 8356−8359.

9 B. J. Trześniewski and W. A. Smith, *J. Mater. Chem. A*, 2016, **4**, 2919−2926.

10 T. W. Kim and K.-S. Choi, *J. Phy.Chem.Lett.*, 2016, **7**, 447−451.

11 Q. Wang, J. He, Y. Shi, S. Zhang, T. Niu, H. She, Y. Bi and Z. Lei, *Appl.Catal. B: Environ.*, 2017, **214**, 158−167.

12 Q. Wang, T. Niu, L. Wang, C. Yan, J. Huang, J. He, H. She, B. Su and Y. Bi, *Chem. Eng. J.*, 2018, **337**, 506−514.

13 S. Wang, T. He, J.-H. Yun, Y. Hu, M. Xiao, A. Du and L. Wang, *Adv. Funct. Mater.*, 2018, **28**, 1802685.

14 Y. Hu, Y. Wu, J. Feng, H. Huang, C. Zhang, Q. Qian, T. Fang, J. Xu, P. Wang, Z. Li and Z. Zou, *J. Mater. Chem. A*, 2018, **6**, 2568−2576.

15 S. Wang, P. Chen, Y. Bai, J. H. Yun, G. Liu and L. Wang, *Adv Mater*, 2018, **30**, 1800486.

16 Y. Q. Tang, R. R.Wang, Y. Yang, D. P. Yan and X. Xu, *ACS Appl. Mater. Interfaces*, 2016, **8**, 19446−19455.